RSC Advances

This is an *Accepted Manuscript*, which has been through the Royal Society of Chemistry peer review process and has been accepted for publication.

Accepted Manuscripts are published online shortly after acceptance, before technical editing, formatting and proof reading. Using this free service, authors can make their results available to the community, in citable form, before we publish the edited article. This *Accepted Manuscript* will be replaced by the edited, formatted and paginated article as soon as this is available.

You can find more information about *Accepted Manuscripts* in the Information for Authors.

Please note that technical editing may introduce minor changes to the text and/or graphics, which may alter content. The journal's standard Terms & Conditions and the Ethical guidelines still apply. In no event shall the Royal Society of Chemistry be held responsible for any errors or omissions in this *Accepted Manuscript* or any consequences arising from the use of any information it contains.

ROYAL SOCIETY OF CHEMISTRY

www.rsc.org/advances

Please do not adjust margins

Journal Name

ARTICLE

Low temperature grown ZnO:Ga films with predominant *c*-axis orientation in wurtzite structure demonstrating high conductance, transmittance and photoluminescence

Received 00th January 20xx,
Accepted 00th January 20xx

DOI: 10.1039/x0xx00000x

www.rsc.org/

Debajyoti Das* and Praloy Mondal

The Ga doped ZnO films grown at a low substrate temperature ~50 °C and a low RF power ~50 W in RF magnetron sputtering possess a predominant *c*-axis orientation in wurtzite structure with $I_{<002>}/I_{<101>}$ ~ 40 in the XRD pattern; which has been further supported by the most prominent presence of the allowed Raman active A_1 *(LO)* mode. The reduced oxygen vacancy in the ZnO network has been correlated to the enhanced optical transparency while the sharp increase in the presence of metallic Ga in the network identified from the XPS data has been attributed to the increasing electrical conductivity of the films prepared at lower temperature. Associated UV luminescence arises as a result of the typical exciton emission or near-band-edge emission, i.e., due to recombination of photo-generated electrons with holes in the valence band or in traps near the valence band. Highly conducting and optically transparent ZnO:Ga film with dominant *c*-axis orientation, demonstrating intense UV–luminescence are extremely useful for many optoelectronic devices including in solar cells, particularly when prepared at such a low substrate temperature most compatible for their fabrication.

Introduction:

ZnO is one of the most interesting direct band gap semiconductors having the optimum electrical and optical properties as well as high melting point of 2248 K and large bond strength cohesive energy of 1.89 eV. Because of having high band gap of 3.37 eV and high exciton binding energy of 60 meV, it has been emerged as a very attractive material for applications in optical devices such as blue, violet and ultraviolet (UV) light emitting diodes (LEDs) and laser diodes (LDs).[1] It has specific advantages such as low cost, nontoxicity, and high stability in hydrogen plasma.[2] Synchronized occurrence of low resistivity and high transmittance of ZnO films in the visible spectrum has made it useful in a variety of potential applications, such as transparent conducting electrodes for flat panel displays[3] and solar cells[4,5], similar to other transparent conducting semiconductors e.g., tin oxide[6,7] and tin doped indium oxide.[8] Doped ZnO thin films combine further low resistance with high transparency; Al, In and Ga have been reported as an effective n–type dopant for intrinsic ZnO thin films.[9-11] Recently, the Ga-doped ZnO thin film has drawn special attention as Ga seems to behave as perfect substitutional dopant for Zn. It is generally known that the electrical and optical properties of Ga-doped ZnO thin films are most favorable as the covalent bond lengths of Ga–O and Zn–O are nearly equal and Ga is less reactive and more resistant to oxidation compared to Al.[12]

ZnO:Ga thin films have been prepared by different techniques, e.g., CVD (chemical vapor deposition), thermal evaporation, MOCVD (metal organic chemical vapor deposition), sol-gel method, etc.[13-16] Considering the application in flat panel displays such as TFT-LCDs (thin film transistor-liquid crystal display) and TCO (transparent conducting oxide) layer in silicon solar cells the sputtering method on glass substrates is most adaptable for the industrial needs as it maintains film uniformity over large area and high deposition rate.[17-19] Substrate temperature is one of the most influential parameters in controlling the optical, electrical and microstructural properties of the films. However, it needs to be sufficiently low in view of the successful integration of the material to different multilayered device structures and in order to make various inexpensive substrates suitable for manufacturing of the devices.

In this study we demonstrate the development of transparent and conducting ZnO:Ga thin films, using the RF magnetron

* *Nano-Science Group, Energy Research Unit,*
Indian Association for the Cultivation of Science,
Jadavpur, Kolkata – 700 032, India.
E-mail (D. Das): erdd@iacs.res.in ; Fax: +91(33)24732805

RSC Advances Accepted Manuscript

sputtering, having preferred crystallographic orientation with controlled morphology and defect profile at low growth temperature and low RF power. The photoluminescent properties have been correlated to its favoured *c*-axis orientation and compositional characteristics, particularly the oxygen vacancies and metallic Ga attached to ZnO lattice, extracted from X-ray photoelectron spectroscopy and Raman spectroscopy.

Experimental:

ZnO:Ga thin films were prepared by RF magnetron sputtering with Ar as the sputtering gas and by using a high purity (99.99%) 2% Ga doped ZnO target. Ar flow rate (~3.3 SCCM) was controlled by a mass-flow controller. The substrate temperature (T_S) was varied from 50 to 300 °C and RF power and pressure was kept fixed at 50 W and 20 mTorr, respectively. The system was evacuated to ~$9x10^{-7}$ Torr prior to deposition and to improve the film homogeneity, the substrate was rotated at 10 rpm by using a rotary driver during deposition. Samples were deposited on Corning® Eagle2000™ glass substrates.

The optical transmission of the films prepared on glass substrate was measured using a Hitachi 330 double-beam spectrophotometer. The X-ray diffraction analysis was carried out using a conventional Cu-Kα X-ray radiation (λ ~1.5418 Å) source and Bragg diffraction setup (Seifert 3000P). The surface morphology of the films were studied by a JEOL JSM-6700F field emission scanning electron microscope (FESEM) and VeecodI CP II (model no - 0100) atomic force microscope (AFM). Room-temperature electrical conductivity measurements were carried out on films prepared on glass by four-probe method. Raman spectra of the samples were taken from a Renishaw inVia Raman Microscope with an excitation wavelength of 514 nm from an air-cooled Ar^+ laser source, at a power density of ~2 mW cm^{-2}. The emission spectra of all samples were obtained with FluoroMax-P (HORIBA JobinYvon) luminescence spectrophotometer. All the fluorescence spectra were recorded at an excitation wavelength of 370 nm at room temperature. The X-ray photoelectron spectroscopy (XPS) of the film was performed using a focused monochromatized Al-Kα X-ray source (1486.8 eV) in the XPS instrument (Omicron Nano Technology 0571).

Results:

X-ray diffraction:

The X-ray diffraction spectra of the ZnO:Ga films prepared at different temperature are shown in Fig. 1(a). The evolution of several number of peaks have been identified at 2θ =31.7º, 34.4º, 36.2º, 47.3º, 56.6º, 62.9º and 67.8º, corresponding to the <100>, <002>, <101>, <102>, <110>, <103> and <112> crystallographic planes of ZnO, respectively. It has been carefully noted that with the increase in the growth temperature the <100>, <101>, <102>, <110> and <112> peaks gradually appear even with a very small intensity at T_S= 200 °C, where the remaining two peaks <002> and <103> also maintain a very

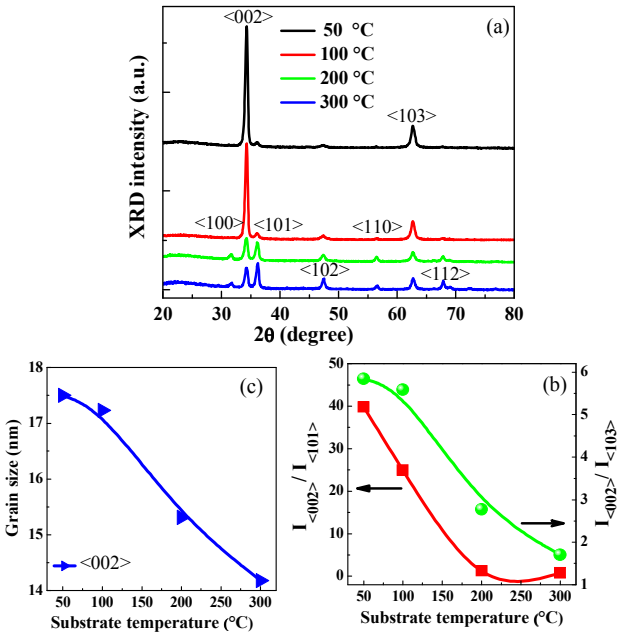

Fig. 1 (a) X-ray diffraction spectra of ZnO:Ga films prepared by magnetron sputtering at different T_S varying from 50 to 300 °C. (b) shows the changes in the intensity ratio, $I_{<002>}/I_{<101>}$ and $I_{<002>}/I_{<103>}$, and (c) the grain size along <002> direction with applied T_S.

low magnitude. However, with the decrease in the growth temperature the latter two peaks grow with rapidly enhanced intensity, the <002> directional growth being significantly dominant at a substrate temperature T_S= 100 °C or lower. At low temperature only <002> and <103> peaks are dominant. The nature of increasing relative intensity $I_{<002>}/I_{<101>}$ and $I_{<002>}/I_{<103>}$ on lowering T_S has been demonstrated in Fig. 1(b), identifying an overall preferential growth of the material along the <002> crystallographic orientation at lower substrate temperature.[18,19] A substantial *c*-axis orientation of ZnO:Ga crystallites grown at T_S= 50 °C appears to be significantly notable.

The average grain size (*D*), has been estimated from the FWHM (β) of <002> peak in the XRD spectra, using Scherer's formula:

$$D = 0.9\,\lambda\,/\beta\,cos\theta,$$

and has been plotted in Fig. 1(c). The *c*-axis orientated ZnO:Ga crystallites of average size ~17.5 nm grows at close to room temperature, T_S= 50 °C which appears significantly useful in device fabrication. The preferred orientation in film growth for materials with a hexagonal structure as ZnO:Ga is governed, in general, by the lowest surface energy of the crystal plane, which extends along <002> direction in the present case.

Optical absorption:

The optical density data of the samples were obtained from the transmission spectra of the ZnO:Ga films, as shown in Fig. 2. It was found that all the samples attained a reasonably high transmission from 85% to 94% at visible range. Fig. 2 identifies that the visible transmittance T_{vis} gradually reduces from ~94 to

RSC Advances Accepted Manuscript

This journal is © The Royal Society of Chemistry 20xx

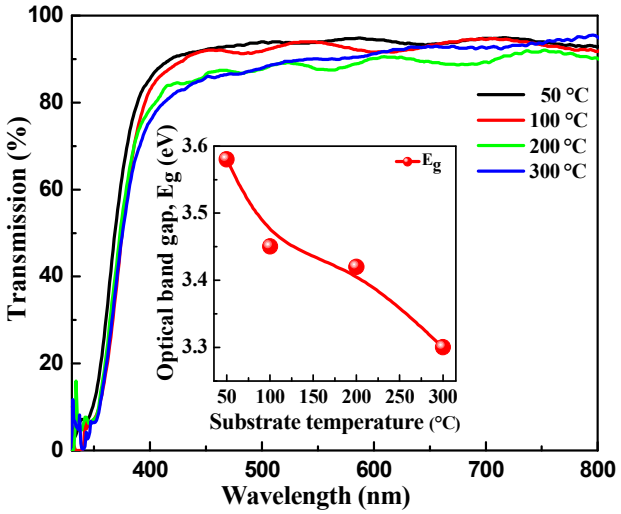

Fig. 2 Optical transmission spectra of ZnO:Ga thin films prepared at different substrate temperatures.

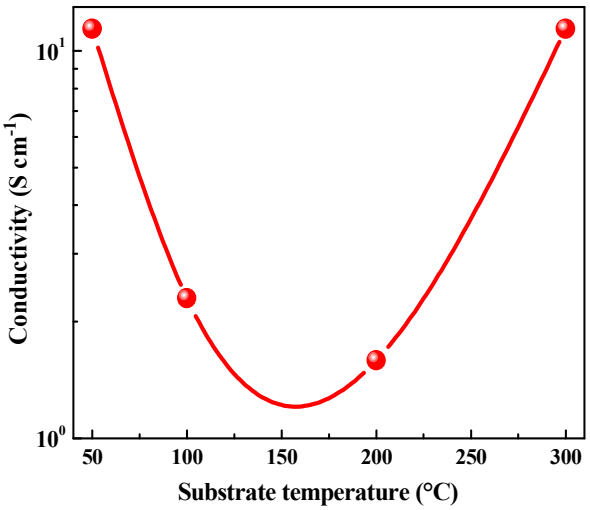

Fig. 3 Electrical conductivity of the ZnO:Ga films prepared at different substrate T_S.

~85% for samples prepared at substrate temperatures increasing from 50 °C to 300 °C.

The optical absorption coefficient, α, has been estimated from:

$$\alpha = 2.303 \times (A/t)$$

where A is the absorbance and t is the thickness of the film. The sharp decrease of transparency of the films in the UV region is caused by the fundamental light absorption within the samples. When scattering effects are neglected, the absorption coefficient could be expressed by the following Tauc's relation

$$\alpha.E = A.(E - E_g)^n$$

where E is the photon energy, A is an energy-independent constant, and n is an exponent which can assume different values depending on the nature of the electronic transitions responsible for the optical absorption, e.g., n= 0.5 and 1.5 for direct allowed and forbidden transitions, respectively, n= 2 and 3 for indirect allowed and forbidden transitions, respectively. As ZnO is a direct band gap material, value of n is taken as 0.5 and E_g is determined from the Tauc plot, as the energy at which the extrapolated linear part of $(\alpha.\cdot E)^2$ vs E plot intersects the energy axis. The variation of E_g with applied substrate temperatures has been shown in the inset of Fig. 2. E_g was found to have the highest magnitude, 3.58 eV at T_S = 50 °C and that gradually reduced to 3.30 eV with increase in T_S to 300 °C. The reduction in the band gap, by ~0.3 eV, might occur due to the increase of oxygen vacancy related disorder causing enhanced band bending effect within the materials at elevated T_S.[20]

Conductivity:

The electrical conductivity of the ZnO:Ga films, as calculated by Van der Pauw method, has been plotted as a function of varying substrate temperature to the plasma, as shown in Fig. 3. The room temperature conductivity (σ) of the film grown at T_S =50 °C was ~11.4 S cm^{-1} that decreased gradually to ~2.3 S cm^{-1} and 1.6 S cm^{-1} with the increase of T_S to 100 °C and 200 °C, respectively. However, on further increase in T_S to 300 °C conductivity again increased to a large extent at σ = 10 S cm^{-1}.

The increase of the crystallite size and the improvement of the crystallinity are, in general, responsible for the decrease of the resistivity due to diminishing grain boundary scattering. Presently, the larger grain size and higher crystallinity with intense preferential orientation along the *c*-axis contributes to the highest conductivity ~11.4 S cm^{-1} at T_S =50 °C. These large size grains of compact structure, in particular, creates enough surface roughness that helps to improve the light scattering from the surface of the ZnO:Ga film which is crucial for its efficient use in thin-film silicon solar cells. The room temperature conductivity attains a maximum 10 S cm^{-1} at T_S =300 °C, probably due to the presence of increased oxygen vacancy within the network, as observed by X-ray photoelectron spectroscopy discussed later.

Raman study:

ZnO films in wurtzite structure belong to the space group C_{6v}^4 with two formula units in the primitive cell. Each Zn atom is tetrahedrally coordinated to four O atoms and vice versa. From the calculations of the group theory, the optical symmetry modes: $\Gamma = A_1 + 2B_1 + E_1 + 2E_2$, could present the lattice optical phonons at the centre of the Brillouine zone. The polar A_1 and E_1 modes exhibit different frequencies for the transverse-optical (TO) and longitudinal-optical (LO) phonons. The E_1 (LO) mode is allied with the presence of oxygen vacancies, interstitial Zn or their complexes. The nonpolar E_2 modes have two frequencies, namely, E_2^{high} and E_2^{low} which are associated to the motion of oxygen atoms and zinc sublattice, respectively.[21] Strong E_2^{high} mode characterizes the wurtzite lattice and indicates good crystallinity. The B_1 modes are silent in Raman scattering.

In Fig. 4, the Raman spectra for the ZnO:Ga films prepared at different T_S exhibit two sharp peaks at 275 cm^{-1} and 580 cm^{-1} which correspond to ($B_1^{high} - B_1^{low}$) mode and A_1 *(LO)* mode of ZnO:Ga films, respectively.[22] In addition, a small peak appeared at 437 cm^{-1} which is assigned to the E_2^{high} mode, as reported from *ab initio* calculations.[23]

RSC Advances Accepted Manuscript

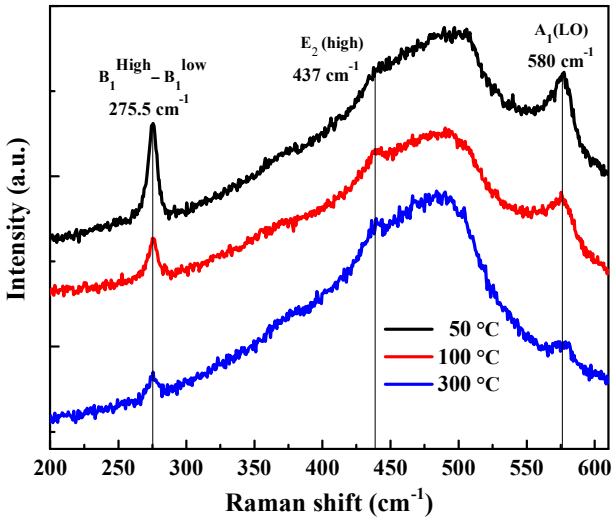

Fig. 4 Raman spectra of the ZnO:Ga films prepared at different substrate T_S.

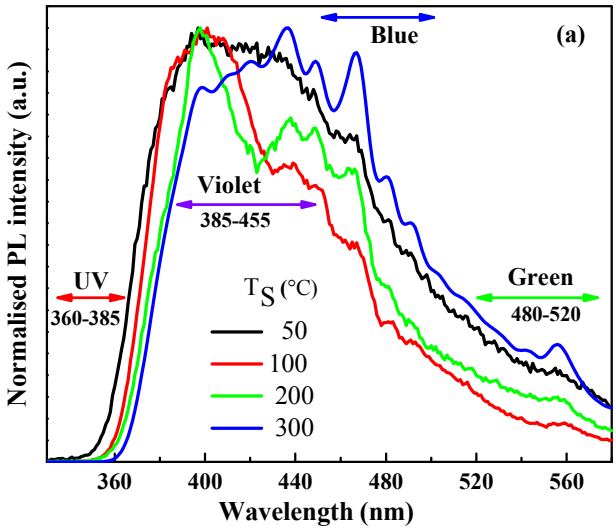

Fig. 5 The normalized photoluminescence spectra of the ZnO:Ga films prepared at different substrate temperatures varying from T_S = 50 °C to 300 °C

It has been observed that the intensity of both the peaks ($B_1^{high} - B_1^{low}$) mode and A_1 *(LO)* mode of the ZnO:Ga films gradually decreases with increase in temperature from 50 °C to 300 °C. Although B_1 mode is Raman inactive, the cause behind the appearance of the second order difference mode ($B_1^{high} - B_1^{low}$) is likely due to disorder-activated Raman scattering. Such scattering is generally induced by the breakdown of the translation symmetry of the lattice caused by defects or impurities showing dopant nature.[24] Because of the differences in mass between dopant Ga and Zn atom this additional mode discussed above are related to intrinsic host lattice defects, which either become activated as vibrating complexes or their concentration increases upon dopant incorporation. A_1 *(LO)* mode appears only when the *c*-axis of wurtzite ZnO:Ga remains parallel to the incident light. Among the possible Raman-active phonon modes in the hexagonal ZnO crystal with wurtzite structure, according to Raman scattering selection rule in the first-order spectra, only the E_2 and A_1 *(LO)* modes are predicted to be observable in backscattering configuration with the photon wave vector parallel to the *c*-axis of the crystal i.e., the incident light normal to the sample surface, used herein.[25] For the polar A_1 *(LO)* mode, the scattering cross-section depends not only on the deformation potential but also on the Fróhlich interaction in materials.

Photoluminescence:

Fig. 5 shows the normalized photoluminescence spectra of the ZnO:Ga films prepared at different substrate temperatures varying from T_S = 50°C to 300 °C, while the spectrum for 50°C has been demonstrated separately in Fig. 6 with possible deconvoluted satellite components. The PL spectra of ZnO:Ga films consist of the UV emission originated from excitonic recombination corresponding to the near band-gap emission of ZnO, while the deep level (DL) emissions in the violet, blue, and green spectral regions are due to the recombination of photo-generated holes with various structural defects e.g., ionized charge states of intrinsic defects, oxygen vacancies, Zn interstitials, zinc vacancies, oxygen antisites, etc. Deconvolution of the visible spectrum identified the distinct presence of several individual components which have been categorized as the UV-violet section at ~395 nm, violet at ~423 nm, violet-blue fragment at ~ 458 nm, blue emission at ~500 nm and a green emission around ~501 nm with a span over 540–560 nm. Increasing concentration of defects in the films prepared at higher substrate temperatures could result in the enhancement of defect emission band in the visible region. The comparatively weak UV emission and strong visible emission band in PL spectra for the material grown at high temperature at T_S =300 °C is consistent with its increasing oxygen vacancies.

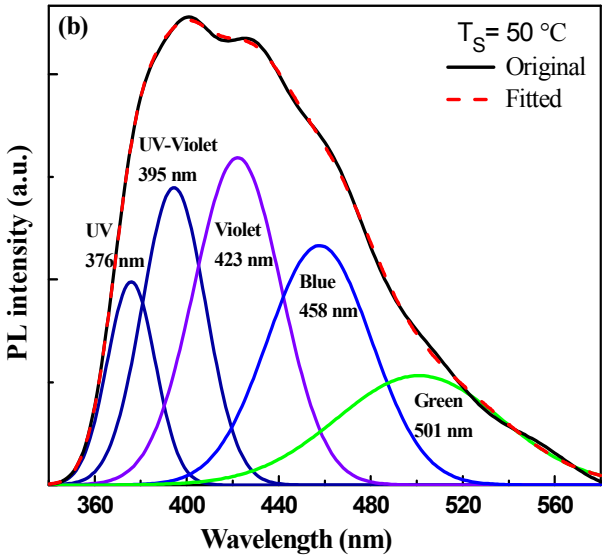

Fig. 6 Possible deconvoluted satellite components of the ZnO:Ga films for T_S =50°C.

RSC Advances Accepted Manuscript

This journal is © The Royal Society of Chemistry 20xx

The UV luminescence bands in the ZnO films depend strongly on surface band bending and those are created from recombination of bound excitons (BEs) complex located near the surface and grain boundaries within the films. There are two factors which directly affect the UV emission in ZnO films. One is the DLE (deep level emission) recombination centres and the other is the non-radiative recombination centers that can degrade the UV emission. The UV emission at ~377 nm that identifies direct band to band transition, is most prominent at an optimum T_S =50 °C, demonstrating better crystalline quality of the sample that has been recognized by its dominant *c*-axis orientation, as identified by XRD studies. However, on increase in substrate temperature, the visible emission that has mostly the defect origin is becoming proportionally significant. The intensity of the visible emission band is, in general, much higher than that of the exciton emission band. Conversely, the intensity under visible band increases when the other band reduces, indicating both emission processes to compete with each other. At elevated substrate temperatures to 300 °C, out diffusion of oxygen from the ZnO:Ga network creates enough oxygen vacancies, demonstrating prominent green emission in photoluminescence. However, in order to account for the systematic relative increase in intensity of different components in the visible region, change in the chemical composition of the material at elevated temperature could be a significant parameter.

X-Ray Photoelectron Spectroscopy:

X-ray photoelectron spectra were taken for the high-resolution scan of Zn, Ga, and O atoms. The binding energies were calibrated with respect to the C1s peak at 284.6 eV. The deconvolutions of the XPS spectrum for core level Zn 2p3/2 of ZnO:Ga film prepared at TS = 50 °C, 100 °C and 300 °C are represented in Fig. 7. A good fit to the experimental data is obtained with two deconvoluted Gaussian components for all the films. The observed peak at the binding energy of 1022 eV is associated to Zn 2p3/2 species in stoichiometric ZnO:Ga film. The core level Zn 2p1/2 XPS spectrum of the film shows a Gaussian component at 1045 eV which correspond to the Zn 2p1/2 species in ZnO matrix. An energy separation of 23 eV between two core level Zn 2p components makes out a good agreement with the literature values for ZnO film.[26,27]

The chemical states of Ga in Ga doped ZnO films are investigated by XPS peaks for Ga $2p_{3/2}$ states as shown in Fig. 8. Ga 2p3/2 peaks can be decomposed into subpeaks; denoted as Ga–Ga (at 1115.5 eV), Ga–Zn (at 1117.7 eV), Ga–O (at 1118.6 eV) and Ga–OH (at 1120.1 eV) which are attributed to metallic gallium, Ga3+ ion substituting Zn^{2+} ion in ZnO lattice, Ga^{3+} ion in oxide phase and hydroxide phase respectively.[28,29] One interesting feature in Fig. 8 is that there are small satellite peaks or shoulders in the lower binding energy side of Ga $2p_{3/2}$ peaks located at 1115.5 eV positions, i.e. 1eV lower than Ga $2p_{3/2}$ peaks, which are attributed to the presence of elemental Ga for the ZnO:Ga film. With increase in T_S from 50 °C to 300 °C the intensity of this peak gradually decreases indicating that at higher temperature the amount of metallic Ga decreases.

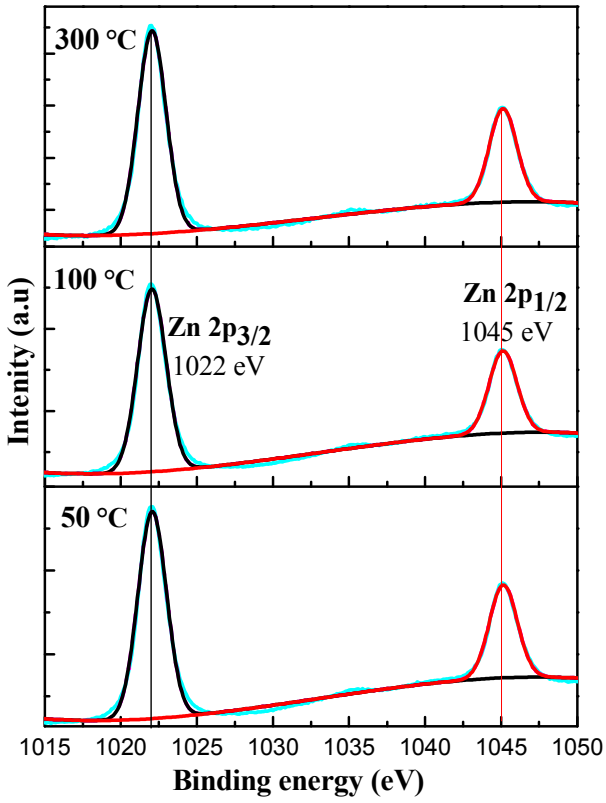

Fig. 7 The Deconvoluted XPS spectrum for core level Zn 2p states of ZnO:Ga films prepared at T_S = 50 °C, 100 °C and 300 °C.

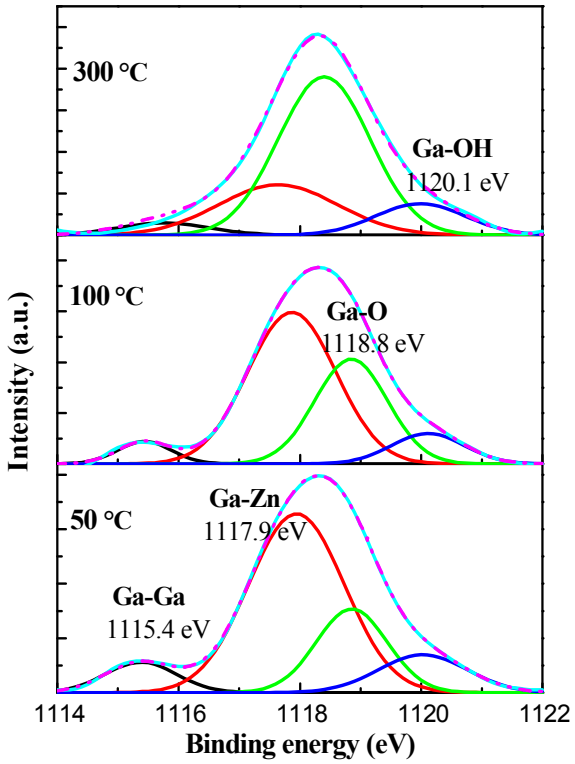

Fig. 8 The chemical states of Ga in Ga doped ZnO films are investigated by XPS peaks for Ga $2p_{3/2}$ states.

RSC Advances Accepted Manuscript

However, the Ga–O and Ga–OH peak intensity increases with increase in temperature, i.e., elevated growth temperature facilitates Ga to preferably detach from both itself (Ga) and Zn and favorably make bonds with O and OH in the film structure.

It is found from Fig. 9 that O1s core level peaks of the films have asymmetric shapes which could be fitted by three nearly Gaussian peaks, centered at ~530.75 eV, 531.8 eV and ~533.1 eV, for all the films prepared at different T_S. Among the three well identified Gaussian components, the lower two binding energy components are identified as due to two types of O^{2-} ions, namely O_I and O_{II}, while the third component appearing at highest binding energy at ~533.1 eV is attributed to the presence of –OH bonds attached to Zn ions on the surface of the films.[30] Such a double oxygen 1s peak was common for oxides containing cations in multiple valence states. It was suggested that the O_I^{2-} ions had neighboring atoms with their full complement of six nearest neighbor O^{2-} ions in the ZnO lattice i.e., the wurtzite structure of ZnO[31], and that the O_{II}^{2-} ions were in oxygen-deficient regions within the matrix of ZnO.[32] Therefore, the changes in the relative intensity of O_{II}/O_I were connected to the variations in the concentration of oxygen vacancies. The relative intensity of O_{II}/O_I has been found to increase significantly for increasing the applied substrate temperature T_S from 50 °C to 300 °C which identifies the formation of a considerable amount of oxygen vacancies in the ZnO:Ga network at high temperature of the growth surface.

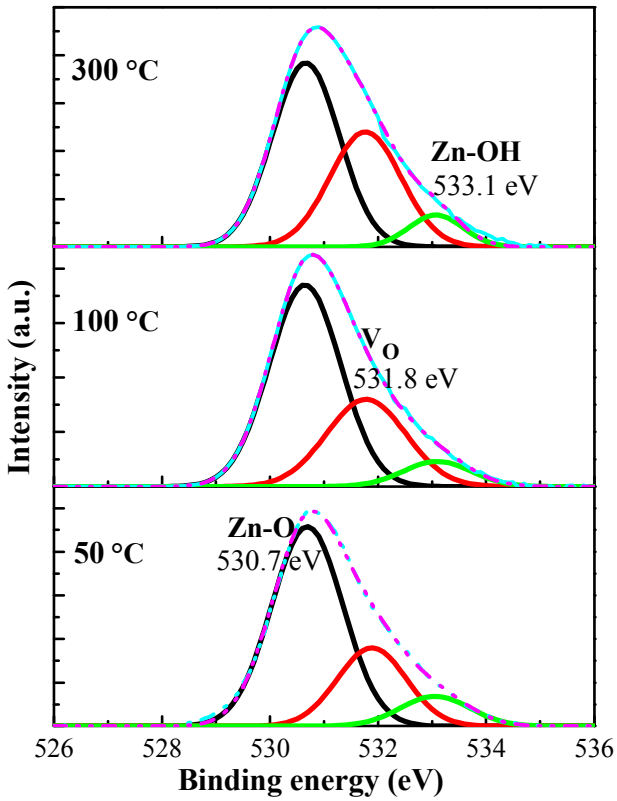

Fig. 9 The O1s core level peaks of the ZnO:Ga films made at different T_S.

Careful observation on the XPS O 1s spectra demonstrates that increasing substrate temperature applied to the sputtering target leads to the growth of ZnO:Ga films wherein the chemisorbed oxygen desorbs from the film surface and the oxygen vacant states increases within Zn lattice interstitials. The increase in O_I and decrease in O_{II} sub-peaks at T_S = 50 °C seem to be related to the reduction of Ga_2O_3 to increase the metallic Ga in the ZnO:Ga film which causes for the improvement of *c*-axis orientation.

SEM:

The typical surface morphologies of ZnO:Ga films prepared at different substrate temperatures were examined by FESEM, as shown in Fig. 10. At T_S =50 °C, the film surface exhibited dense morphology. The compact surface texturing originates due to the nucleation of oriented *c*-axis grains that grows geometrically and impinges each other laterally. Large crystal agglomerates do possess well identified but closely connected boundaries, providing a highly packed surface. The overall solid structure was formed due to anisotropic growth of various crystal facets of wurtzite ZnO:Ga film. At T_S =200 °C, crystal agglomerates became slightly larger in size, got connected intermittently and the compact surface texturing grossly reduced, as the *c*-axis orientation diminished significantly. However, at T_S =300 °C, the surface texture was grossly different with lots of visible pores and a loosely bound texture on the surface which appears distinctly in the image. The significantly different surface morphology could be correlated to the radical change in growth morphology from *c*-axis orientation towards dominant <101> orientation at high temperature to the plasma.

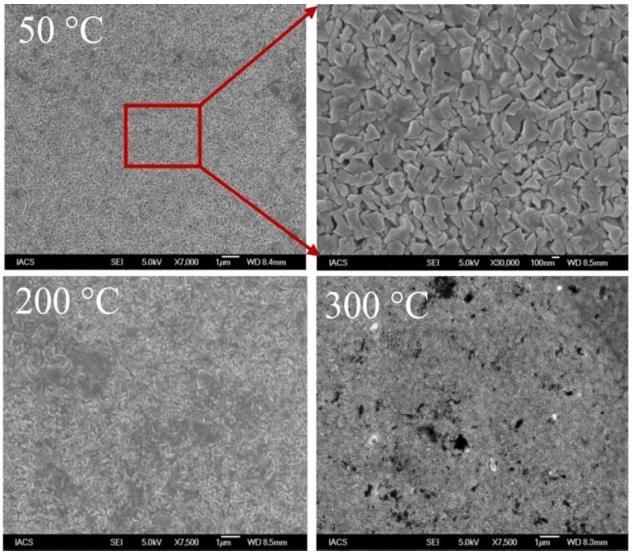

Fig. 10 The typical surface morphologies of ZnO:Ga films prepared at different substrate temperatures. The magnified part of the ZnO:Ga film prepared at substrate temperature 50 °C is also shown.

RSC Advances Accepted Manuscript

This journal is © The Royal Society of Chemistry 20xx

Discussion:

The XRD pattern revealed that the as-deposited ZnO:Ga films were polycrystalline with a hexagonal structure, and had a preferred orientation with the *c*–axis perpendicular to the substrate. The <002> diffraction angle was close to that of the standard ZnO crystal (34.421, JCPDF#36-1451), and no metallic Zn characteristic peak or no characteristic peaks of other impurities was observed in the pattern. Beside the <002> and <103> diffraction peaks increased uninterruptedly whose relative intensity $I_{<002>}/I_{<103>}$ increased monotonously, the <101> peak reduced significantly leading to a notable increase in $I_{<002>}/I_{<101>}$, as the applied substrate temperature reduced systematically. Indeed, the XRD patterns show a clear change of the growth direction, from a preferential orientation along the <101> crystallographic plans to a crystallographic orientation along the <002> plane, leading to a change of $I_{<002>}/I_{<101>}$ from <1 to ~ 40 for lowering of T_S from 300 to 50 °C. This abrupt transition in the crystallographic preferential growth direction is accompanied with a morphological change of the growing surface, as observed in the SEM micrographs of the ZnO films surface. At an elevated substrate temperature the growth of the ZnO layers became less ordered, with the apparition in the XRD of multiple growth orientations. At low substrate temperature (50 °C) due to the presence of metallic Ga the mobility of the particles on the substrate increases and that allows the atoms to find places of minimum energy on the substrate surface before the next layer is deposited, yielding to preferred *c*-axis oriented crystallographic growth perpendicular to the substrate surface.

The shift of the preferred crystallographic orientation from <002> to <101> could be explained by the change in the incorporation of Ga compounds in the ZnO crystal along with the oxygen vacancy created at higher temperature. With increasing substrate temperature, the circulation of sputtering species like Ga_2O_3, $Ga(OH)_3$ etc is enhanced and the grains oriented towards <101> direction as the gallium ions substitute the zinc ions that forms an additional kind of gallium sites within ZnO:Ga films.[33-36] The ionic radius of trivalent Ga^{3+} (0.062 nm) is much smaller than that of divalent Zn^{2+} (0.074 nm). This causes the shifting of diffraction peaks to higher angle in order to satisfy the Bragg's law. In addition at higher temperature there is the formation of higher oxygen vacancies (V_O) at tetrahedral or octahedral sites that distorts the octahedral symmetry. As a result gallium ion will then be easily incorporated in the Zn site of the ZnO:Ga films. However, there is a slight increase in FWHM and grain size becomes smaller when the substrate temperature exceeds 100 °C. This fact implies the substrate temperature have a remarkable effect on the structure of ZnO:Ga; high crystalline ZnO:Ga films required optimum substrate temperature e.g., 50 °C in this case.

When the incident light is parallel to the *c*-axis of ZnO samples, the Raman active E_2 modes and A_1 *(LO)* modes are allowed, whereas A_1 *(TO)* and E_1 *(TO)* modes are forbidden, according to Raman selection rules. In case of the present Raman measurement, the incident light is exactly perpendicular to the samples surface. For the present set of samples, in general, A_1 *(LO)* modes are distinctly present in the Raman spectrum which identifies that ZnO films are of fairly Wurtzite structure. In addition, strong Raman band demonstrates the most favoured *c*-axis orientation of the hexagonal ZnO crystalline structures prepared at an optimum T_S = 50 °C, which has been equitatively supported by the results e.g., a very high magnitude of $I_{<002>}/I_{<101>}$~ 40, obtained from X-ray diffraction studies.

The Raman inactive mode (under normal conditions) at 275 cm^{-1} occurs due to defects created in host lattice by the introduction of Ga ions within the films.[37,38] In the present case the formation of metallic Ga results in the breaking of local translational symmetry and enhances the scattering events at low substrate temperature 50 °C.

The increase of the grain size and the improvement of the crystallinity are, in general, responsible for the decrease of the resistivity by virtue of increasing carrier mobility due to diminishing grain boundary scattering. The enhanced conductivity in the case of ZnO:Ga film prepared at higher temperature at T_S =300 °C is due to the increase in the concentration of carriers supplied from the substituted Ga atoms which get ionized into Ga^{3+}, making free electrons available. In addition, at higher substrate temperature formation of higher oxygen vacancies (V_O) at tetrahedral or octahedral sites, as observed by O 1S XPS spectra, distort the octahedral symmetry and donate electrons, thereby increasing conductivity. In case of the ZnO:Ga films prepared at a low substrate temperature of 50 °C the presence of metallic Ga attached to Zn lattice, as revealed by XPS studies, helps increasing the mobility, simultaneously facilitating a dominant *c*-axis orientation. Dense morphology of the film surface reduces the weak localization effect on charge carriers and improves the electrical conductivity.

Fig. 11 represents a comparative study correlating room temperature electrical conductivity with the optical band gap, among various ZnO:Ga films deposited by different processes, as reported from contemporary literature.[39-44]

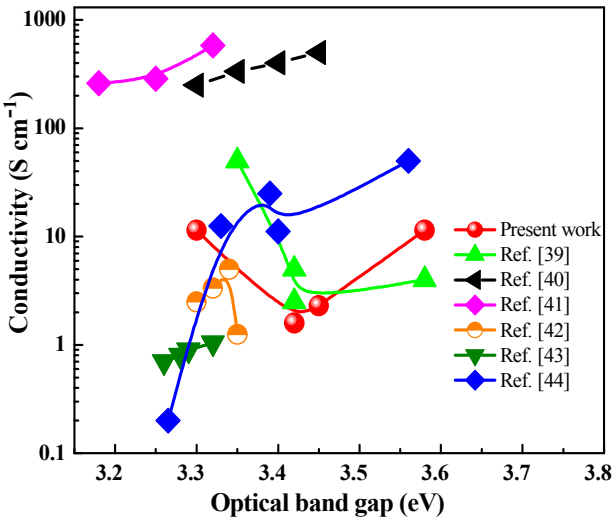

Fig. 11 A comparative study, correlating room temperature electrical conductivity and optical band gap, among various works reported on the development of ZnO:Ga films deposited by different processes.

RSC Advances Accepted Manuscript

It has been identified that in some of the cases, the conductivity is encouragingly high; however, the optical band gaps are limited within 3.45 eV. Among the relatively wider optical band gaps, the high conductivity of the ZnO:Ga films reported by Khranovskyya et al.,[44] is obtained from the PEMOCVD process on substrate placed on a heated holder that does not specify the deposition temperature. In this regard, dark electrical conductivity ~11.4 S cm^{-1} of the ZnO:Ga films having a wide optical band gap ~3.58 eV prepared at a low substrate temperature T_S =50 °C by RF magnetron sputtering, as reported by the present manuscript, appears reasonably encouraging both from the point of view of device compatible growth temperature and growth technology, as well.

The luminescence emission properties are extremely sensitive to the defect states in ZnO. Emissions in the visible range (violet, blue, green, yellow, and orange-red) are likely due to donor acceptor transitions involving the point defects such as vacancies of oxygen and zinc, interstitial oxygen and zinc, antisite oxygen, as well as other extrinsic impurities in ZnO:Ga.[45-48] In spite of many investigations on the luminescent properties a consensus about the origins of defect-related visible emissions has not been reached due to the complexity of the microscopic details. The visible emission over a wide energy range around 380–560 nm could be nicely deconvoluted into different satellite components in each case, as shown in Fig. 6. Analysis on the possible origin of individual component has been made from the available energy positions of various defect centres existing within Zn–O system. In ZnO:Ga films the UV–violet emission (~395 nm) is ascribed to possible electron transition from the conduction band to single ionized oxygen vacancy (V_O^+). The violet luminescence (~423 nm) may appear through possible transition of electrons trapped at Zn interstitial (Zn_i) defects to the valence band.[19] The blue emission (~458 nm) is due to a radiative transition of electrons from the Zn vacancy (V_{Zn}) to holes in the valence band. The green emission (~501 nm) originates when the photo-generated holes trapped in the deep level oxygen vacancy (V_O) recombine with the electrons trapped in a shallow level located just below the conduction band.[49-52] The intensity UV emission confirms the high quality of the ZnO:Ga film prepared at T_S as low as 50°C.

Addition of Ga^{3+} into the ZnO:Ga film is expected to modify the energy band structure of ZnO:Ga film which affects the optical properties of ZnO:Ga film. The intermediate impurity levels within optical band gap region generated by defects determine the emission features of the ZnO film. The dopant Ga influences intrinsic defect states of intrinsic ZnO film notably. Experimentally and theoretically it is found that dopant Ga induces V_{Zn} in ZnO:Ga film due to self–charge compensation.[53] Moreover, Ga can also occupy both substitutional (Ga_{Zn}) and interstitial sites (Ga_i) of ZnO:Ga crystal.[54] At higher temperature due to larger Ga compound concentration, vacancy complexes such as Ga_{Zn}–V_{Zn} and Ga_{Zn}–O_i are formed due to strong Coulomb interaction. These complexes affect mainly deep acceptor states of the ZnO:Ga film. This is the reason for which the intensity of the blue peak at 463 nm increases sharply at higher temperature 300 °C due to the presence of more V_{Zn} as this peak arises due to a radiative transition of an electron from the shallow donor level of Zn_i to an acceptor level of neutral Zn vacancy (V_{zn}).

The XPS results revealed the ZnO:Ga films grown at higher temperature is non-stoichiometric which can contain many defects in the lattice or the surface. The UV emission is associated to the excitonic recombination corresponding to the near band-edge transition, where as the visible emission band is commonly attributed to the defects on the surface or in the bulk of the material. Increasing concentration of defects in the films prepared at higher temperature could result in the enhancement of defect emission band in the visible region. The weak UV emission and strong visible emission band in PL spectra for the material grown at high temperature, T_S = 300 °C, is consistent with its increasing oxygen vacancies which might have stronger influence than the reducing metallic Ga attached to Zn lattice. Careful observation on the XPS O 1s and Zn 2p spectra demonstrates that increasing substrate temperature leads to the growth of ZnO:Ga films where in the chemisorbed oxygen desorbs from the film surface and the oxygen vacant states increases within Zn lattice interstitials.

Presence of metallic Ga attached to Zn lattice, as revealed by XPS studies, could be correlated to the dominant *c*-axis orientation at T_S = 50 °C, corresponding to distinct UV luminescence exhibited by the material. While the increased oxygen vacancy at higher temperatures (~300 °C) keeps on favouring the growth along <101> crystallographic orientation which might be correlated to increased visible emission, particularly the luminescence in green and blue region.

The photo excitation and the emission phenomena in the present scenario for the ZnO:Ga film can then be summarized as follows, along with a schematic presentation in Fig. 12:[19]

i) UV emission band around 376 nm arising due to the typical exciton emission or near-band-edge emission.

ii) UV-violet emission peak at 399 nm, attributed to possible electron transition from the conduction band to single ionized oxygen vacancy (V_O^+), as the responsible acceptor defects located at 0.27 eV above the valence band.

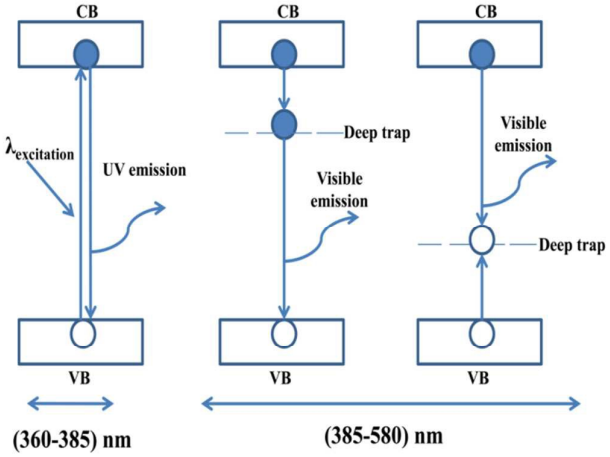

Fig. 12 Schematic band diagram, demonstrating various PL emission components originated due to electronic transitions between different defect levels and the band edges of ZnO:Ga films, prepared by RF magnetron sputtering system.

RSC Advances Accepted Manuscript

This journal is © The Royal Society of Chemistry 20xx

iii) The violet luminescence peak at 427 nm appearing through possible transition of electrons trapped at Zn interstitial (Zn_i) defects to the valence band.

iv) Radiative recombination of electrons from the neutral Zn vacancy (V_{Zn}) to holes in the valence band leads to the evolution of blue component of PL peak located at around 460 nm.

v) An emission band around 554 nm arising when the photogenerated holes trapped in the deep level oxygen vacancy (V_O) recombine with the electrons trapped in a shallow level located just below the conduction band.

Conclusion:

The ZnO:Ga film prepared at RF power 50 W and at a low temperature 50 °C possess a very good conductivity 11.4 S cm^{-1} and a high transmission ~95% within visible range. The increase in the crystallite size and the improvement of the crystallinity with preferred *c*-axis orientation helps to increase the conductivity by diminishing grain boundary scattering. These grains of compact structure, in particular, creates enough surface roughness that helps to improve the light scattering from the surface of the ZnO film which is crucial for its efficient use in thin-film silicon solar cells. The XRD spectra demonstrated the <002> peak as of highest intensity for the sample prepared at T_S = 50 °C, identifying its preferential *c*-axis orientation relative to another prevailing growth along <101> direction that appeared gradually dominant at higher T_S. The preferred orientation in film growth for materials with a hexagonal structure as ZnO is governed, in general, by the lowest surface energy of the crystal plane, which extends preferentially along <002> direction i.e., along the *c*-axis at a low substrate temperature ~50 °C, in the present case. The shift of the preferred crystallographic orientation from <002> to <101> at elevated substrate temperature could be explained by the change in the introduction of Ga compounds incorporation in the ZnO crystal and creation of oxygen vacancy. Raman study revealed the presence of strong A_1 *(LO)* mode that supports the preferred *c*-axis orientation. In addition, the presence of strong ($B_1^{high} - B_1^{low}$) modes, which usually are Raman inactive, suggest the relaxation of the Raman selection rules due to the breaking of the local translational symmetry of the crystal lattice by incorporation of Ga ions.

The XPS results revealed the as-grown films as non-stoichiometric which can contain many defects in the lattice or the surface. Presence of substantial amount of metallic Ga attached to Zn lattice, at T_S = 50 °C, could be correlated to the dominant *c*-axis orientation of the ZnO crystals which exhibited distinct UV luminescence band that arises as a result of the typical exciton emission or near-band-edge emission, i.e., due to recombination of photo-generated electrons with holes in the valence band or in traps near the valence band. Addition of Ga^{3+} into the ZnO:Ga film produces more V_{Zn} so the intensity of blue peak increases sharply at higher temperature 300 °C. In addition to increasing oxygen vacancies in neutral (V_O) and ionized (V_O^+) states, a number of other defects are generates, which include Zn interstitial (Zn_i, Zn_i^+), neutral ionized Zn vacancy (V_{Zn}) and oxygen antisite (O_{Zn}) as the dynamic acceptor defects which act as the defect origins of different visible photoluminescence components classified in the UV-violet, violet, violet-blue, blue and green regions. Intense UV–luminescence and visible emission of the ZnO:Ga film prepared at T_S =50 °C are extremely useful for many optoelectronic devices along with its regular use as TCO layers in solar cells.

Acknowledgement:

The work has been done under nano-silicon projects funded by Department of Science and Technology (Nano-Mission Program) and Council of Scientific and Industrial Research, Government of India.

Notes and references

1. A. Tsukazaki, A. Ohtomo, T. Onuma, M. Ohtani, T. Makino, M. Sumiya, K. Ohtani, S. F. Chichibu, S. Fuke, Y. Segawa, H. Ohno, H. Koinuma and M. Kawasaki, *Nature Mater*., 2005, **4**, 42–46.
2. Ü. Özgür, Ya. I. Alivov, C. Liu, A. Teke, M. A. Reshchikov, S. Doğan, V. Avrutin, S. J. Cho and H. Morkoç, *J. Appl. Phys.*, 2005, **98**, 041301.
3. T. Minami, *Semicond. Sci. Technol.*, 2005, **20**, S35–S44.
4. A. K. Barua, A. Sarker, A. K. Bandyopadhyay, D. Das and S. Ray, Proceedings of 28th IEEE Photovoltaic Specialists Conference, (Anchorage Alaska, USA, September 17-22, 2000) pp. 829-832.
5. T. Shinagawa, K. Shibata, O. Shimomura, M. Chigane, R. Nomura and M. Izaki, *J. Mater. Chem. C*, 2014, **2**, 2908-2917.
6. D. Das and R. Banerjee, *Thin Solid Films,* 1987, **147**, 321–331.
7. R. Banerjee and D. Das, *Thin Solid Films*, 1987, **149**, 291–301.
8. R. Banerjee, D. Das, S. Ray, A. K. Batabyal and A. K. Barua, *Solar Energy Materials*, 1986, **13**, 11–23.
9. S. B. Zhang, S. H. Wei and A. Zunger, *Phys. Rev. B,* 2001, **63**, 075205.
10. J. Hu and R. G. Gordon, *Mater. Res. Soc. Symp. Proc.,* 1993, **283**, 891.
11. H. J. Ko, Y. F. Chen, S. K. Hong, H. Wenisch, T. Yao and D. C. Look, *Appl. Phys. Lett.,* 2000, **77**, 3761-3763.
12. H. C. Park, D. Byun, B. Angadi, D. H. Park, W. K. Choi, J. W. Choi and Y. S. Jung, *J. of Appl. Phys.,* 2007, **102,** 073114.
13. S. Chen, G. Carraro, D. Barreca, A. Sapelkin, W. Chen, X. Huang, Q. Cheng, F. Zhange and R. Binions, *J. Mater. Chem. A,* 2015, **3**, 13039–13049.
14. T. Nama, C. W. Lee, H. J. Kima and H. Kim, *Appl. Surf. Sci.,* 2014, **295**, 260–265.
15. S. Kuprenaite, T. Murauskas, A. Abrutis, V. Kubilius, Z. Saltyte and V. Plausinaitiene, *Surf. Coat. Technol.,* 2015, **271**, 156–164.
16. S. Chen, M. E. A .Warwick and R. Binions, *Sol. Energy Mater. Sol. Cells.,* 2015, **137**, 202–209.
17. G. Xiong, J. Wilkinson, B. Mischuck, S. Tüzemen, K. B. Ucer and R. T. Williams, *Appl. Phys. Lett*., 2002, **80**, 1195–1197.
18. P. Mondal and D. Das, *Appl. Surf. Sci.*, 2013, **286**, 397–404.
19. D. Das and P. Mondal, *RSC Adv.*, 2014, **4**, 35735-35743.
20. S. Dutta, S. Chattopadhyay, D. Jana, A. Banerjee, S. Manik, S. K. Pradhan, M. Sutradhar and A. Sarkar, *J. Appl. Phys.,* 2006, **100**, 114328.
21. X. Li, Y. Wanga, W. Liu, G. Jiang and C. Zhu, *Mater. Lett.,* 2012, **85**, 25–28.
22. J. Serrano, A. H. Romero, F. J. Manjo`n, R. Lauck, M. Cardona and A. Rubio, *Phys. Rev. B*, 2004, **69**, 094306.
23. F. J. Manjón, B. Marí, J. Serrano and A. H. Romero, *J. Appl. Phys*., 2005, **97** , 053516.
24. C. Bundesmann, N. Ashkenov, M. Schubert, D. Spemann, T. Butz, E. M. Kaidashev, M. Lorenz and M. Grundmann, *Appl. Phys. Lett.*, 2003, **83**, 1974–1976.

RSC Advances Accepted Manuscript

25. C. L. Du, Z. B. Gu, M. H. Lu, J. Wang, S. T. Zhang, J. Zhao, G. X. Cheng, H. Heng and Y. F. Chen, *J. Appl. Phys*., 2006, **99**, 123515.
26. J. F. Moulder, W. F. Stickle, P. E. Sobol and K. D. Bomben, Handbook of X-ray Photoelectron Spectroscopy, Perkin-Elmer Corporation, Eden Prairie, 1992.
27. C. D. Wagner, A. V. Naumkin, A. Kraut-Vass, J. W. Allison, C. J. Powell and J. R. J. Rumble, NIST X-ray Photoelectron Spectroscopy Database, Default.aspx, (accessed November 2012) U.S. Secretary of Commerce, 2007
28. C. L. Hinkle, M. Milojevic, B. Brennan, A. M. Sonnet, F. S. Aguirre–Tostado, G. J. Hughes, E. M. Vogel and R. M. Wallace, *Appl. Phys. Lett.*, 2009, **94,** 162101.
29. F. Mitsugi, Y. Umeda, N. Sakai and T. Ikegami, *Thin Solid Films*, 2010, **518**, 6334–6338.
30. E. De la Rosa, S. Sepu´lveda-Guzman, B. Reeja-Jayan, A. Torres, P. Salas, N. Elizondo and M. J. Yacaman, *J. Phys. Chem. C*, 2007, **111**, 8489–8489.
31. N. S. Ramgir, D. J. Late, A. B. Bhise, M. A. More, I. S. Mulla, D. S. Joag and K. Vijayamohanan*, J. Phys. Chem. B*, 2006, **110**, 18236–18242.
32. Fan J. J. C and Goodenough J. B, *J. Appl. Phys*., 1977, **48**, 3524–3531.
33. A. S. Gonçalves, S. A. M. Lima, M. R. Davolos, S. G. Antônio and C. O. P. Santos, *J. Solid State Chem.,* 2006, **179**, 1330–1334.
34. M. J. Lee, J. Lim, J. Bang, W. Lee and J. M. Myoung, *Appl. Surf. Sci.*, 2008, **255**, 3195–3200.
35. K. T. R. Reddy, H. Gopalaswamy and P. J. Reddy, *J. Cryst. Growth*, 2000, **210**, 516-520.
36. B. H. Choi, H. B. Im, J. S. Song and K. H. Yoon, *Thin Solid Films*, 1990, **193**, 712-720.
37. M. Gaba´ s , P. D-Carrasco, F. A-Rueda, P. Herrero, A. R. L-Ca´novas and J. R. R-Barrado, *Sol. Energy Mater. Sol. Cells.,* 2011, **95**, 2327–2334.
38. F. Friedrich and N. H. Nickel, *Appl. Phys. Lett.*, 2007, **91**, 111903.
39. W. S. Liu, W. K. Chen and K. P. Hsueh, *J. Alloys Compd*., 2013, **552,** 255–263.
40. S. Liang and X. Bi, *J. Appl. Phys*., 2008**, 104**, 113533.
41. Y. Li, Q. Huang and X. Bi, *J. Appl. Phys*., 2013**, 113**, 053702.
42. S. Kim, J. Seo, H. W. Jang, J. Bang, W. Lee, T. Lee and J. M. Myoung, *Appl. Surf. Sci*, 2009, **255**, 4616–4622.
43. P. K. Nayak, J. Yang, J. Kim, S. Chung, J. Jeong, C. Lee and Y. Hong, *J. Phys. D: Appl. Phys*., 2009, **42,** 035102.
44. V. Khranovskyya, U. Grossner, V. Lazorenko, G. Lashkarev, B. G. Svensson and R. Yakimova, *Superlattices Microstruct*., 2006, **39**, 275–281.
45. L. P. Li, X. Q. Qiu and G. S. Li, *Appl. Phys. Lett.*, 2005, **87**, 124101.
46. X. L. Wu, G. G. Siu, C. L. Fu and H. C. Ong, *Appl. Phys. Lett.*, 2001, **78**, 2285–2287.
47. M. K. Patra, K. Manzoor, M. Manoth, S. R. Vadera and N. Kumar, *J. Lumin.*, 2008, **128**, 267–272.
48. S. Shi, J. Xu, X. Zhang and L. Li, *J. Appl. Phys.*, 2011, **109**, 103508.
49. A. van Dijken, E. A. Meulenkamp, D. Vanmaekelbergh and A. Meijerink, *J. Phys. Chem. B*, 2000, **104**, 1715–1723.
50. L. Zhang, Y. Longwei, C. Wang, N. Lun, Y. Qi and D. Xiang, *J. Phys. Chem*. C, 2010, **114**, 9651–9658.
51. Q. Zhu, C. Xie, H. Li, C. Yang, S. Zhang and D. Zeng, *J. Mater. Chem. C*, 2014, **2**, 4566–4580.
52. C. Magne, T. Moehl, M. Urien, M. Gr¨atzelc and T. Pauport´e, *J. Mater. Chem. A*, 2013, **1**, 2079-2088.
53. D. C. Look, K. D. Leedy, L. Vines, B. G. Svensson, A. Zubiaga, F. Tuomisto, D. R. Doutt and L. Brillson, *Phys. Rev. B*., 2011, **84**, 115202.
54. D. O. Demchenko, B. Earles, H. Y. Liu, V. Avrutin, N. Izyumskaya, U¨. O¨zgu¨r and H. Morkoç, *Phys. Rev. B*., 2011, **84**, 075201.

RSC Advances Accepted Manuscript

 This journal is © The Royal Society of Chemistry 20xx

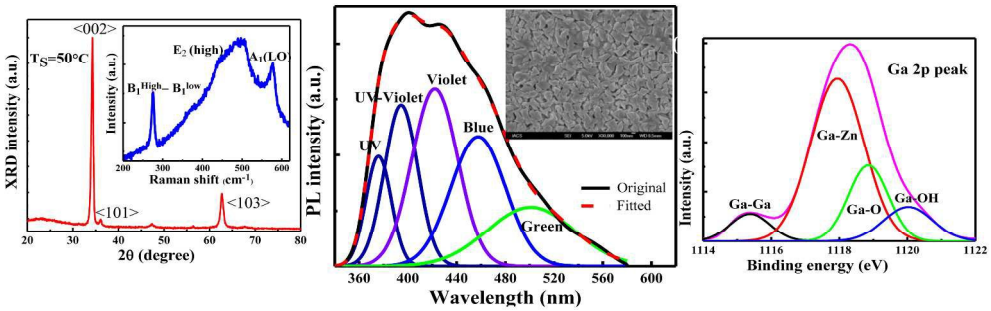

253x86mm (300 x 300 DPI)

RSC Advances Accepted Manuscript